JOURNAL OF SPACECRAFT AND ROCKETS
Vol. 47, No. 4, July–August 2010

Miniaturized Optical Sensor for Leak Detection in a Space Environment

John E. Sinko,* Valentin Korman,† and Adam Hendrickson‡
Kratos Defense and Security Solutions, Huntsville, Alabama 35805
and
Kurt A. Polzin§
NASA Marshall Space Flight Center, Huntsville, Alabama 35812

DOI: 10.2514/1.46693

A miniature optical, laser-based, interferometric leak detector is presented for application as a means to detect on-orbit gas leaks. The sensor employs a fiber-coupled modified Michelson interferometer to detect gas leaks by measuring an increase in gas density in the sensing region. Monitoring changes in the fringe pattern output by the interferometer allows for direct measurement of the gas density in the sensing region and, under the assumption of an equation of state, this can be used to obtain a pressure measurement. Measurements obtained over a pressure range from 20 mtorr to 760 torr using a prototypical interferometer on working gases of air, nitrogen, argon, and helium generally exhibit agreement with a theoretical prediction of the pressure increase required before an interference fringe completely moves over the detector. Additional measurements performed on various gases demonstrate the range of detectable species, measuring subtorr pressure changes in the process. Time-resolved data prove the capability of this sensor to detect fast gas flow phenomena associated with transients and pressure waves.

Nomenclature

A	=	molar refractivity, cm^3/mol
l	=	path length difference, cm
m	=	order of interference
N	=	particle density, m^{-3}
N_A	=	Avagadro's number (particles per mol)
n	=	index of refraction
P	=	pressure, torr
R	=	universal gas constant ($J\,K^{-1}\,mol^{-1}$)
T	=	temperature, K
α	=	bulk polarizability, cm^3
λ	=	wavelength, nm
μ	=	instrument sensitivity (torr per fringe)
ϕ	=	phase, rad

I. Introduction

LONG-TERM storage of volatile liquids and high-pressure gases in space is now seen as a necessary step for facilitating safe space travel to celestial objects such as the moon or Mars. Examples of such mission-critical fluids include cryogenic fuels and oxidizers, high-pressure gases supporting mechanical systems or propulsion, and life-support consumables such as oxygen. Successful storage of such fluids in a space environment is essential for mission success, despite the significant challenges. A leak in a storage or distribution system can cause a variety of problems, including mission-endangering loss of inventory or unbalanced thrust loads on the vehicle. Long-term storage of cryogenic propellants presents a special challenge. The propellant can boil off and be lost through the insulating walls of the tank, or simply escape during thermal cycling of the fittings, valves, and propellant feed lines, when seals are unseated.

Current NASA missions anticipate long-duration in-space storage of propellants, oxidizers, and life-support supplies. Leaks of a scale detectable through a pressure drop in the storage tank are often catastrophic and have long been the focus of ground-based mitigation efforts where redundant systems are often employed. However, there is presently no technology available for detecting and monitoring low-level, but still mission-endangering, gas leaks in space. Standard in-space gas detection methods are limited either by their operational pressure range or by selective detection of only certain gases. For example, vacuum gauges typically have defined pressure ranges of less than 10^{-3} torr or greater than 10^{-3} torr, but cannot cover both ranges with a single instrument. However, depending on the severity of the leak and the relative distance between the leak and the sensor, the pressure could span orders of magnitude in pressure, making it difficult to use a single type of gauge for these measurements. Mass spectrometer systems are able to perform detection tasks, but their size, mass, and use of high voltage, which can potentially cause arcing and ignition of combustible propellants, severely limit their usefulness in space systems. In addition, most of these measurements are not time-accurate and integrate over a relatively large volume.

In this paper, we present a light-based interferometric approach to gas monitoring and leak detection using a fiber optic coupled, interferometric leak detector sensor. The output of the sensor is the intensity at a point in the interference fringe pattern, which is a function of the gas density (and thus the bulk index of refraction) in the sample region. Changes in the density of gas in the test region cause corresponding changes in the intensity output onto a photodiode detector. This process provides a real-time, temporal history of a leak. The sensor is fiber coupled and constructed from solid optics, allowing for placement almost anywhere on a spacecraft and for stable, rugged operation, respectively. The sensor consumes very little power (in principle, operation at around 100 mW input power is realizable), and does not introduce an ignition source.

The outline for the rest of this paper is as follows. In Sec. II, a theoretical treatment of the sensor is presented showing how different gases will affect the output of a sensor. The design of the fiber-coupled sensor tested for this paper is given in Sec. III. The

Presented as Paper 2009-5394 at the 45th AIAA/ASME/SAE/ASEE Joint Propulsion Conference & Exhibit, Denver, CO, 2–5 August 2009; received 11 August 2009; revision received 30 March 2010; accepted for publication 9 April 2010.

*Madison Research Division, Optics Research Scientist.
†Madison Research Division, Senior Optics Research Scientist.
‡Madison Research Division, Optics Research Scientist.
§Propulsion Research Engineer, Propulsion Research and Technology Applications Branch, Propulsion Systems Department; kurt.a.polzin@nasa.gov. Senior Member AIAA (Corresponding Author).

experimental setup used to test the sensor is described in Sec. IV. Finally, testing results are presented in Sec. V and a few specific strategies for improving future designs are discussed in Sec. VI.

II. Sensing Theory

The interference of two rays of light is a well-known physical phenomenon [1–3]. Interference is easily understood in the case where the rays each have the same wavelength and there is a phase difference of $\Delta\phi$ between them, as occurs in a two-path interferometer with a laser light source. For fixed path lengths and for fixed wavelength λ, the order of interference m can be directly related to the index of refraction n between the reference and signal path lengths. Change in the index of refraction will directly result in a change in the interference order, leading to a fringe shift:

$$\Delta m = \frac{\Delta\phi}{2\pi} = \frac{l\Delta n}{\lambda} \tag{1}$$

where l is the difference between the signal and reference path lengths.

An actual interferometer sensor must include a reference path and a signal path. The beams traveling on these two paths recombine (i.e., interfere) before detection. A longer signal path length will increase l resulting in a higher value of m. Because the index of refraction for any gaseous material approaches unity as density is lowered to zero, the sensor must be very sensitive, or it will not be able to observe leaks at low density levels.

The index of refraction n of a medium and the particle density N are related by the Lorentz–Lorenz relation [1]:

$$N = \frac{3}{4\pi\alpha}\frac{n^2-1}{n^2+2} \tag{2}$$

where α is the bulk polarizability. For an ideal gas, the density may be alternatively expressed as a pressure P:

$$P = \frac{3}{4\pi}\frac{RT}{\alpha N_A}\frac{n^2-1}{n^2+2} \tag{3}$$

where R is the universal gas constant, T is the temperature, and N_A is Avagadro's number. The bulk polarizability can be defined in terms of the molar refractivity A, typically given in units of $\mathrm{cm}^3/\mathrm{mol}$:

$$A = \frac{4\pi}{3}N_A\alpha \tag{4}$$

Values of A are given in the literature for a variety of gases, a few of which are presented in Table 1. A change in the value of the molar refractivity of the test gas will significantly affect the performance of a fiber optic leak detector sensor. In addition, the sensor should be more sensitive to specific species based on their refractivities. This trait will be discussed in more detail below.

Table 1 Molar refractivity values for selected gases

Gas	Molar refractivity, A, $\mathrm{cm}^3/\mathrm{mol}$	T, K	Source
Air	4.606	287.5	[1]
Ar	4.196	282.5	[4]
	4.1973 ± 0.0005	298	[5]
	4.207	299	[6]
	4.194	298	[7]
CO_2	6.642	292.6	[4]
	6.650	299	[6]
	6.590	298	[7]
H_2	2.0845 ± 0.0004	298	[8]
He	0.5220	287.7	[4]
	0.5210 ± 0.0002	303	[9]
Kr	6.377	292.6	[4]
N_2	4.446	292.5	[4]
	4.460	299	[6]
	4.446	298	[7]
	4.458	298	[8]
	4.4454 ± 0.0005	298	[10]
Ne	1.003	292.5	[4]
O_2	4.028	292.5	[4]

The measurement of interest relies on the ability to discriminate between two pressure values (or density values) by examining the fringe movement; it must relate a change in pressure (density) to the movement of fringes past the photodetector. (Note: throughout this paper, we refer mostly to changes in pressure because that quantity is more easily measurable by independent means for validation purposes.) By combining Eqs. (1), (3), and (4), assuming near vacuum conditions, $n \approx 1$, and holding λ, T, and l constant, an approximate relationship between the time rate of change of pressure and the rate of change in order can be written as

$$\frac{\partial P}{\partial t} \approx \frac{2RT\lambda}{3Al}\frac{\partial m}{\partial t} \tag{5}$$

Equation (5) is useful, but the real parameter of interest in evaluating the behavior of the sensor is the rate of change in the pressure with respect to the order of interference (hereafter referred to as μ):

$$\mu \equiv \frac{\partial P}{\partial m} \approx \frac{2RT\lambda}{3Al} \tag{6}$$

The parameter μ essentially provides bounds on the limits of sensitivity of the instrument. The integrated result is a linear relationship between the pressure and order. The pressure change per fringe order will decrease with increasing path length and molar refractivity, and increase with increasing temperature and wavelength. In some cases, it may also be useful to consider μ^{-1}. The number of fringes per unit pressure change will directly increase with increasing path length and molar refractivity, and decrease with increasing temperature and wavelength.

The wide range in values of A shown in Table 1 imply that, in principle, it should be possible to detect changes in gas composition within the test region if the gas density (pressure) is otherwise held constant, and the types of gases in the test volume are known. For instance, if the sensor was used to measure pure He instead of pure CO_2, a difference of over an order of magnitude would be observed in the value of μ between the species under the same pressure conditions. A mixture of He and CO_2 would have a mean polarizability somewhere between that of a pure sample of He or CO_2, leading to a molar refractivity bounded by the values for the two species. Given that the species and pressure are known, the intensity of the observed interference fringe would allow for an exact measurement of the ratio of the two gas species present.

III. Sensor Design

The sensor design was aimed at producing a detector that was compact, robust, and sensitive. A longer sensing path length leads to increased sensitivity, but it also increases the overall size of the device. Single mode fiber was used for delivery of the laser light to the sensor. Use of single mode fiber eliminated internal fiber interference between different wave propagation modes, resulting in a sensor output that varied smoothly and uniformly as the interference fringes moved relative to the return (sensor output) fiber optic. For the initial effort described in this paper, simple light interference was used, as opposed to the more complex light beam frequency modulation techniques common to other interferometric sensors. While it is beyond the scope of this paper, the intent of future work would be to increase the sensor's performance by integrating more advanced interferometric methods into the design. Improvements would be aimed at providing a fringe-to-pressure reference point and increasing sensitivity and robustness.

A photograph and schematic of a prototypical lab-model sensor are shown in Fig. 1. In the interferometer, light follows two major paths; a reference path and a sensing path. The sensing path length in the prototype is 6.50 ± 0.05 cm. Light enters through one of the fiber optic cables at right, is collimated by a gradient index (GRIN) lens, and is split by the first beamsplitter. The reference path light

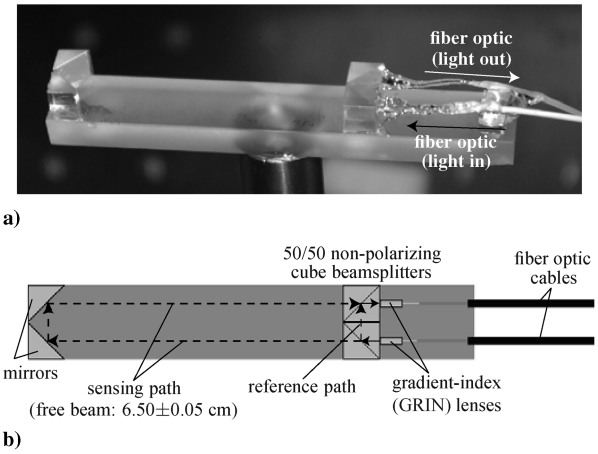

Fig. 1 A fiber-coupled gas detection sensor: a) photograph, and b) schematic.

travels within the two beamsplitters, while the sensing path light transitions to a free beam and passes through a volume of gas. After reflecting off two mirrors, the sensing beam returns to the second beamsplitter where it recombines with the reference beam, producing an interference pattern. The light is focused by a second GRIN lens into a fiber optic cable that leads to a photodiode detector. Changes in the gas within the sensing path region cause the interference pattern produced by the combination of the sensing and reference beams to move, and this motion is detected by the photodiode and correlated into a measurement of gas density (or pressure). For simplicity, the entire sensor was constructed on a rectangular ground glass BK7 base plate.

IV. Experimental Setup

Testing was conducted in the small stainless steel vacuum chamber shown schematically in Fig. 2, which measures approximately 30 cm in diameter and 1 m in length. The chamber was evacuated to a 10^{-3} torr base for the experiments presented in this paper. Light for the sensor is conducted into and out of the chamber using a pair of sealed fiber optic vacuum feedthroughs. The light signal is generated using a 632.8 nm continuous wave HeNe laser with a beam power of 30 mW. In testing, the operation of the sensor

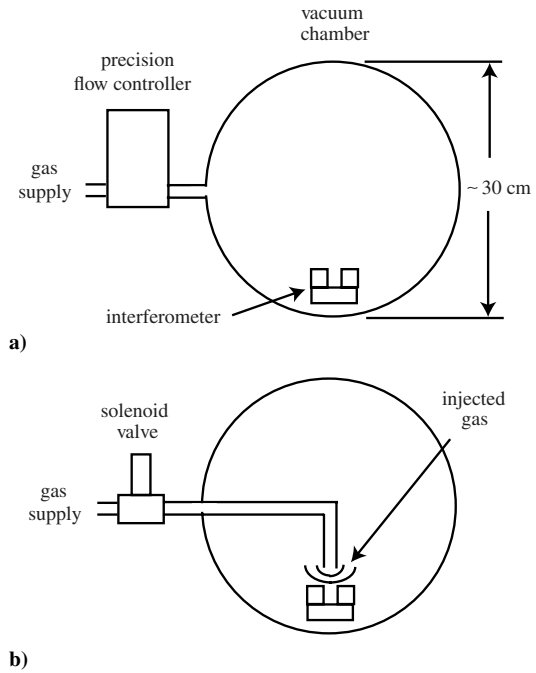

Fig. 2 Schematic of the experimental apparatus used for a) controlled gas injection testing, and b) fast, pulsed gas injection testing.

was found to be roughly independent of the polarization of the laser beam.

Controlled gas injection was performed using an MKS1479 precision flow controller. Testing was conducted by isolating the chamber from its vacuum pumping system and then introducing gas into the chamber at a specified volumetric flow rate. The signal from the sensor was measured using a silicon photodiode. An independent measure of the gas pressure in the chamber was performed using an MKS baratron gauge, which is a gas-independent capacitance manometer pressure gauge. Both the photodiode and baratron voltage outputs were simultaneously recorded to yield a time history of both parameters.

Fast gas injection was performed using a solenoid valve, which was energized for almost a second before being closed. The valve was fed by air at atmospheric pressure, and the flow was directed by a tube with the exit placed just above the sensor. This was done to maximize the gas density at the sensor while minimizing the gas density rise time in the sensing region.

V. Results

The data presented in this section serve to provide an illustrative representation of the capabilities of the sensor in its present form. Notionally, we expect that as the density (or alternatively the pressure) increases, changing the index of refraction of the gas in the sensing path, interference fringes will pass by the detector resulting in the intensity peaks and valleys shown in Fig. 3. Assuming constant temperature and perfect rigidity in the alignment of the interferometer, these peaks should repeat and be indistinguishable from each other.

A. Controlled Gas Injection

Measurements performed to validate the response of the sensor as a function of increasing gas pressure are presented in Fig. 4. These data were obtained using the configuration shown in Fig. 2a. This configuration provided a controllable source of the gas flow rate into the vacuum chamber. Pressure measurements were obtained to correlate the increase in pressure with the number of fringes passing the detector. In all cases, the flow rate was set to 1500 sccm. Gases represented in Figs. 4a–4d were air, nitrogen, argon, and helium, respectively.

The fringe spacings for air, nitrogen, and argon were 26.4, 26.5, and 28.4 torr/fringe, respectively. These data compare favorably with Eq. (6) when the actual sense path length, laser wavelength, and the values of molar refractivity for each gas (Table 1) are used to compute the number of torr per fringe. The data for He is different from the other three sets in two ways. First, there are far fewer fringes over the pressure range tested, which is expected because the molar refractivity is much smaller in this case than for the other three gases tested. Also, the fringe spacing as a function of pressure was not observed to be uniform. This could be an effect of the residual gas that remained in the vacuum chamber after evacuation. At the lower pressure levels the measurement is effectively being performed on a mixture composed of air and helium, with a molar refractivity of the mixture somewhere between the values for either gas. As more helium was injected into the chamber, the response of the system is governed more by the molar refractivity value of pure helium, and the fringe spacing as a function of pressure becomes more uniform.

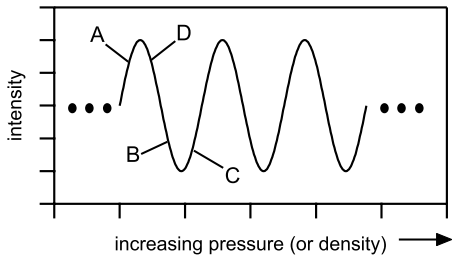

Fig. 3 Plot showing the notional response of the interferometer as a function of increasing pressure and/or density (at constant temperature).

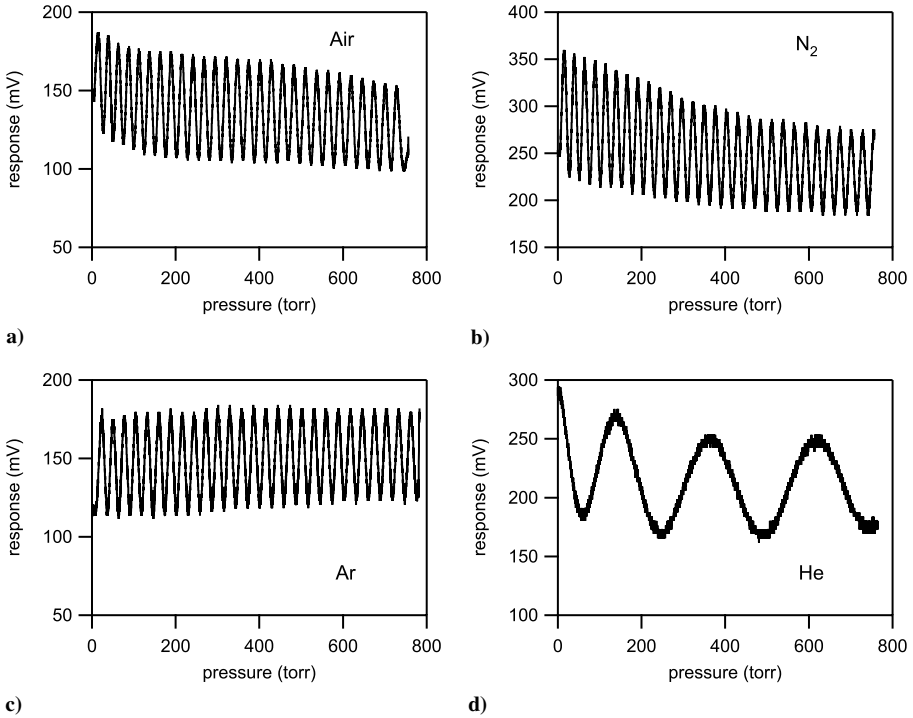

Fig. 4 Interferometer measured response to moving interference fringes as a function of pressure (from 0–760 torr) for a) air, b) nitrogen, c) argon, and d) helium.

Because air, argon, and nitrogen all have similar values of A, this effect did not appear in any noticeable fashion in those data sets.

Additional data are presented in Fig. 5 for air, argon, carbon dioxide, and krypton, showing the interferometer response as a function of increasing pressure, displayed on a semilog scale from a rough vacuum level of $\sim$100 mtorr up to about 10 torr. These data we acquired at a flow rate of 35 sccm to allow for better resolution at the low end of the pressure regime. The difficulty in generating and analyzing these data using the present setup is that the interferometer does not always start at the same point in the interference pattern, so it may be deeper in a valley or nearer to a peak for different trials. However, these data displayed on the semilog axis show the pressure level where the sensor is effective in detecting changes. At these moderate flow rates and for the prototypical sensor used in this study, this sensitivity is well below 1 torr.

B. Fast Gas Injection

Data obtained from fast gas injection testing performed using the configuration shown in Fig. 2b are presented in Figs. 6a–6d for similar gas pulses at acquisition rates of 10, 50, 250, and 500 ksamples/s, respectively. The solenoid valve is opened at time $t = 0$, and closed less than a second later. For these tests, the tank pressure started at $\sim$10 mtorr and ended at 5–10 torr.

In Fig. 6a, the signal from the interferometer first rises quickly, then falls to a lower level, continuing to decrease at a slow rate after the initial transient before reversing and beginning to rise again just after 500 msec. When the valve is closed, there is a slight dip in the signal before it quickly increases back to roughly the initial output level. This pattern can be understood using the notional plot in Fig. 3. In the notional plot, the interferometer's initial output is represented by point A on the curve. As the solenoid valve is energized, the signal quickly rises to the peak level before dropping to the level of point B on the curve. Over the next 800 msec, as the choked flow set up a quasi-steady flowfield with a slightly increasing density in the interferometer sense region, the signal continues to decrease through a valley, reaching point C as the valve is closed. When the valve is closed, interrupting the gas source, the local density at the interferometer decreases again, and the output of the sensor travels backward from C through the interference fringe minimum and up to D. The data in Figs. 6b–6d demonstrate that the sensor has the capability for time-resolved measurements on the order of the response time of the photodiode being employed. In addition, these measurements show that the initial transient behaves in the manner described above.

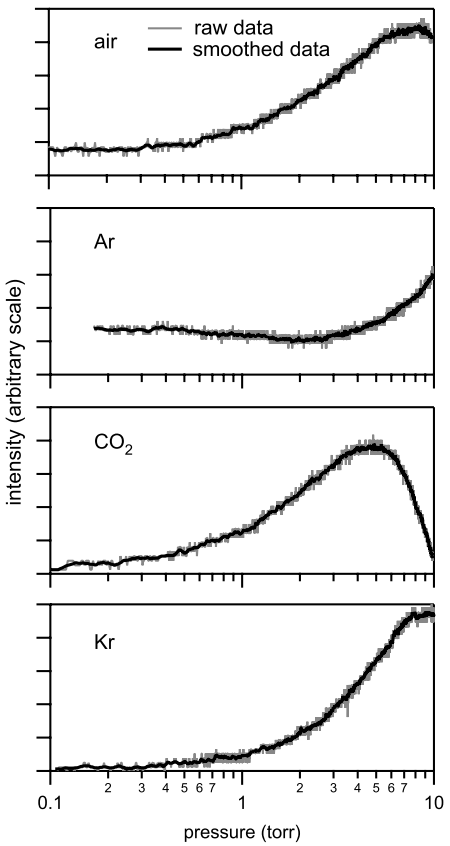

Fig. 5 Interferometer measured response to moving interference fringes as a function of pressure (at low pressure levels displayed on a semilog scale) for air, argon, carbon dioxide, and krypton. The intensity scale spans the same range for all plots.

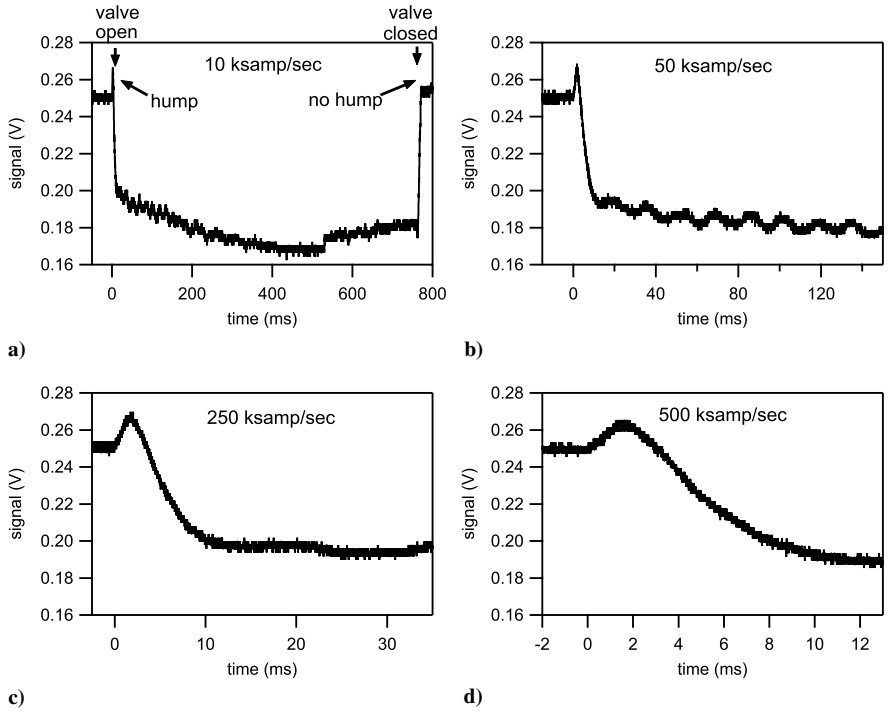

Fig. 6 Interferometer response to a short, fast gas pulse injected at the sensor head acquired at a) 10, b) 50, c) 250, and d) 500 ksamples/s.

Another noteworthy feature in the pulsed gas injection data is observed in Figs. 6a and 6b. At 10 ksamples/s, after the initial transient there is considerable hash in the data, which could be taken to represent noise. However, at 50 ksamples/s, we observe that there is actually a regular, repeating oscillation superimposed on the main signal. The first oscillation and a half appear in the data presented in Fig. 6c and correlate with the commensurate data in Fig. 6b. The oscillations in the data are likely caused by the detection of compression and rarefaction waves passing through the sensing region of the interferometer. These oscillations do not correlate with any AC electrical signal (60 Hz) and have more structure to them than experimental noise. In addition, it is unlikely that the oscillations are due to sensor or mirror vibrations because the optical elements are bonded directly to the base, which is itself relatively thick and rigid.

VI. Specific Future Improvements to the System

Not discussed in this paper are the effects of temperature on the measurement, especially considering that the sensor could be applied to cryogenic gas leakage situations. Future iterations of the sensor will incorporate more advance design features mentioned here or offered by other authors in the field. Of note, the use of low thermal expansion substrate materials (e.g., Zerodur) as well as advanced optical design principles [2] can limit errors associated with thermal drift. Further testing is needed to evaluate the performance of the concept discussed here to quantify the sensitivity in regards to gas-type leak detection, which may occur relatively quickly compared with slower thermal effects.

In the present work, an unamplified Si-photodetector was employed to measure the fringes, and the unfiltered signal was acquired using an oscilloscope operating in a DC-coupled mode. Data acquisition was always performed while the vacuum pumps were off, but no other isolation of the system from outside environmental noise was employed. Filtering the signal or operating in an AC-coupled mode may have allowed for removal of noise from the measurement, and is simple enough to implement on future iterations of this work. Another noise rejection technique that may be employed is to pulse or chop a laser beam above the noise threshold of the system, and then measure the signal using an AC-coupled scope or lock-in amplifier. This would allow filtering below the frequency threshold of the noise while passing the signal through to the data acquisition system, which could be very useful in the thermal environment discussed above or on a launch vehicle where vibrational noise would otherwise prove a large impediment to performing optical leak detection.

VII. Conclusions

On-orbit sensing of gas leaks in mission-critical components and systems can assist in reducing risk and enhancing the overall safety, increasing the probability of mission success. A fiber optic-coupled interferometric leak detection sensor has advantages over other state-of-the-art detection techniques, making it well suited for deployment in space. The fiber-coupled nature of the sensor allows for remote placement near critical areas on a spacecraft. In addition, the sensor is compact, relatively unaffected by many environmental factors, and does not introduce an ignition source into what could be an explosive fuel/oxidizer mixture. Measurements obtained using a prototypical interferometric sensor generally agree favorably with theoretical predictions of the number of torr per fringe over a pressure range from 20 mtorr to 760 torr. Deviations from the theoretical response for helium, especially in the lower pressure regime, can be understood as being a measurement of a gas mixture composed of residual air in the test vessel and injected helium. Plotting the sensor response as a function of the pressure (on a semilog scale) demonstrates a sensitivity on a proof-of-concept apparatus of under 1 torr for most of the gases tested. Pulsed gas-injection data show the ability to use the sensor to acquire fast, time-resolved transient data, capturing not only the bulk pressure variations but also much faster flow oscillation phenomena.

Acknowledgments

We are grateful for the project support provided by the NASA Marshall Space Flight Center Technology Transfer Office. Funding for Madison Research Division Kratos was provided under NASA contract NAS8-02060. We gratefully acknowledge the NASA Marshall Space Flight Center support staff of Tommy Reid, Doug Galloway, and Roger Harper, and undergraduate students Adam Kimberlin, Joe Balla, and Jarred Reneau for their contributions to this effort. We also thank Ben Ramsey, Randy James, and Jason Hughes of Madison Research Division Kratos for their assistance in the fabrication of components used in this study. This work benefitted from several insightful suggestions and comments made by Don

Gregory of the University of Alabama in Huntsville and Kenneth Herren of NASA Marshall Space Flight Center. Finally, we want to thank James Martin and J. Boise Pearson for continued management support of this effort.

References

[1] Born, M., and Wolf, E., *Principles of Optics*, 7th expanded ed., Cambridge Univ. Press, Cambridge, England, 1999.

[2] Hariharan, P., *Basics of Interferometry*, Academic Press, New York, 1992.

[3] Vest, C. M., *Holographic Interferometry*, 1st ed., Wiley, New York, 1979.

[4] Birch, K. P., "Precise Determination of Refractometric Parameters for Atmospheric Gases," *Journal of the Optical Society of America A (Optics, Image Science and Vision)*, Vol. 8, No. 4, 1991, p. 647. doi:10.1364/JOSAA.8.000647

[5] Coulon, R., Montixi, G., and Occelli, R., "Experimental Determination of the Refractivity Viral Coefficients for Argon Gas," *Canadian Journal of Physics*, Vol. 59, No. 10, 1981, p. 1555.

[6] Buckingham, A. D., and Graham, C., "The Density Dependence of the Refractivity of Gases," *Proceedings of the Royal Society of London, Series A: Mathematical and Physical Sciences*, Vol. 337, No. 1609, 1974, p. 275. doi:10.1098/rspa.1974.0049

[7] Burns, R. C., Graham, C., and Weller, A. R. M., "Direct Measurement and Calculation of the Second Refractivity Virial Coefficients of Gases," *Molecular Physics*, Vol. 59, No. 1, 1986, p. 41. doi:10.1080/00268978600101901

[8] Diller, D. E., "Refractive Index of Gaseous and Liquid Hydrogen," *Journal of Chemical Physics*, Vol. 49, No. 7, 1968, p. 3096. doi:10.1063/1.1670554

[9] Kirouac, S., and Bose, T. K., "Polarizability and Dielectric Properties of Helium," *Journal of Chemical Physics*, Vol. 64, No. 4, 1976, p. 1580. doi:10.1063/1.432383

[10] Montixi, G., Coulon, R., and Occelli, R., "Refractivity Virial Coefficients for Nitrogen at 25°C," *Canadian Journal of Physics*, Vol. 61, No. 3, 1983, p. 473.

I. Boyd
Associate Editor